International Journal of Heat and Technology
Vol. 41, No. 3, June, 2023, pp. 602-610
Journal homepage: http://iieta.org/journals/ijht

A Computational Fluid Dynamics Study on Polymer Heat Exchangers for Low-Temperature Applications: Assessing Additive Manufacturing and Thermal-Hydraulic Performance

Ahmed M. Alshwairekh

Department of Mechanical Engineering, College of Engineering, Qassim University, Qassim 52571, Saudi Arabia

Corresponding Author Email: shoierkh@qu.edu.sa

https://doi.org/10.18280/ijht.410312

Received: 2 May 2023
Accepted: 21 June 2023

Keywords:
CFD, heat exchangers, low-temperature heat exchangers, 3D printing, Nusselt number, friction factor

ABSTRACT

In this study, a computational fluid dynamics (CFD) model is employed to examine the feasibility of utilizing corrugated polymer-based heat exchangers for low-temperature applications. The k-ω Shear Stress Transport (SST) turbulence model is implemented for simulating turbulent fluid flow within the flow channels in cases with corrugations and varying Reynolds numbers, while a laminar model is applied for the flat heat exchanger cases. The simulations reveal that, under specific conditions, polymer-based heat exchangers exhibit effective heat transfer performance for low-temperature applications. When the heat exchanger's polymer surface thickness is less than 2.7 mm and possesses corrugations, its heat transfer efficiency surpasses that of flat aluminum heat exchangers with the same thickness. Furthermore, the analysis of the thermal-hydraulic performance demonstrates that incorporating small, widely-spaced corrugations on the heat exchanger surface yields optimal heat transfer relative to the increase in pumping power. These encouraging findings emphasize the need for further experimental investigations to validate the performance of corrugated polymer-based heat exchangers in low-temperature applications.

1. INTRODUCTION

1.1 Background information

Heat exchangers (HXs) are essential devices for facilitating heat transfer between two fluids [1]. While the design and operation of HXs are well-established, emerging manufacturing techniques offer new possibilities for their fabrication. In recent years, additive manufacturing (commonly referred to as 3D printing) has garnered significant interest as a promising approach to HX production. Traditionally, HXs are manufactured from highly conductive materials to minimize heat conduction resistance and enhance heat transfer rates. Various methods, such as incorporating turbulators or corrugations within the HXs, can further improve heat transfer rates [2, 3]. However, fabricating HXs with these features can be challenging or even impossible using conventional techniques [4]. Additive manufacturing offers a solution to these difficulties, enabling the design and production of HXs with intricate features in a single step. As 3D printers become more accessible, the cost and manufacturing constraints associated with HX production are likely to decrease [5].

1.2 Literature review

Heat exchangers come in a variety of designs, including shell and tube, plate, spiral, and compact HXs. Numerous studies have explored the use of 3D printing for HX design and fabrication. Haertel et al. [6] investigated polymer filaments filled with conductive metals for constructing 3D-printed HXs, which were employed as condensers in dry-cooled power plants. By optimizing the air-side design of the HX, the researchers identified the ideal combination of conductive metal materials and cell unit height for 3D-printed HX performance. Kim and Yoo [7] introduced a novel method for designing the complex core of compact HXs, which is difficult to achieve using conventional computer-aided design (CAD) packages. Using MATLAB and the volumetric distance field method, the researchers generated intricate geometries for 3D-printed HXs, resulting in ultra-efficient designs with minimal pressure drop. Lowrey et al. [8] fabricated an air-to-air polymer plate heat exchanger using fused deposition modeling and compared its performance to an aluminum counterpart. Under dry conditions, both HXs exhibited similar performance, while the aluminum HX outperformed the polymer version under wet conditions.

Additionally, Puttur et al. [9] developed an innovative lung-inspired, desiccant-coated HX for controlling indoor humidity in buildings. The complex shape of the HX facilitated greater interfacial area between air and desiccant, as well as reduced pressure drop. Experimental results demonstrated that the new design outperformed standard desiccant-coated HXs by a factor of two. Ahmadi et al. [10] created a 3D-printed, lung-inspired ceramic HX for high-temperature applications without gas leakage between hot and cold surfaces. The ceramic 3D-printed HX showed a 71% improvement compared to milli channel HXs.

Computational fluid dynamics (CFD) is a valuable tool for analyzing and studying the flow field within 3D-printed HXs, which often exhibit high heat transfer rates due to complex and turbulent fluid flow. Laitinen et al. [11] developed a 3D-printed aluminum HX and evaluated its performance using both experimental and CFD methods. Employing various

turbulence models, such as k-ε, k-ω SST, and large-eddy simulations (LES), the researchers found that k-ω SST and LES models showed good agreement. Wang et al. [12] proposed a 3D-printed, fractal-tree-like HX and studied its hydrodynamic performance experimentally and numerically. Their results indicated that the fractal tree-like HX achieved high heat transfer rates with low-pressure drop.

Polymer HXs offer several advantages over conventional designs, including lower cost, reduced weight, anti-corrosion, and antifouling properties [13]. When additively manufactured, polymer HXs can achieve large heat transfer surface areas with thin walls and complex flow channels that promote turbulence. However, further study is needed to fully exploit the potential of 3D-printed HXs.

This paper employs a CFD approach to investigate and evaluate a 3D-printed flat plate HX. The primary objective is to examine the effect of polymer-based 3D-printed HXs on heat transfer rates, comparing their performance with aluminum HXs and assessing the impact of mixing promoters or corrugations. Additionally, the results are validated using existing experimental work from the literature.

2. MATHEMATICAL MODEL

The conservation of mass, the conservation of momentum, and the energy equations are solved numerically, and their mathematical form is given as:

The conservation of mass

$$\frac{\partial u_i}{\partial x_i} = 0 \tag{1}$$

The conservation of momentum as:

$$u_j \frac{\partial u_i}{\partial x_j} = -\frac{1}{\rho}\frac{\partial p}{\partial x_i} + \frac{1}{\rho}\frac{\partial}{\partial x_j}\left(\mu \frac{\partial u_i}{\partial x_j}\right) \tag{2}$$

The energy transport equation as follows:

$$u_j \frac{\partial T}{\partial x_j} = \frac{k}{\rho c_p}\frac{\partial}{\partial x_j}\left(\frac{\partial T}{\partial x_j}\right) \tag{3}$$

where, ρ is the fluid density, p is the pressure, μ is the viscosity, T is the temperature, k is the thermal conductivity, and c_p is the specific heat of the fluid inside the HX. u_i is the velocity vector, and i and j are tensorial indices.

Several of the simulated cases for the 3D-printed HX are considered turbulent. The *k-ω* shear stress transport (*k-ω SST*) turbulence model is used [11, 14]. The laminar model can be used for smooth channels of the HX and with low Reynold numbers. However, for the complex shapes of the flow channels and with relatively high Reynold numbers, a suitable turbulence model must be used to capture the effect of large and small eddies and their impact on the thermal-hydraulic performance of the HX. The *k-ω* shear stress transport model equations are given as:

$$u_j \frac{\partial u_i}{\partial x_j} = -\frac{1}{\rho}\frac{\partial p}{\partial x_i} + \frac{1}{\rho}\frac{\partial}{\partial x_j}\left((\mu + \mu_t)\frac{\partial u_i}{\partial x_j}\right) \tag{4}$$

$$u_j \frac{\partial T}{\partial x_j} = \frac{\partial}{\partial x_j}\left(\left(\frac{k}{\rho c_p} + \frac{\mu_t}{\rho\, Pr_t}\right)\frac{\partial T}{\partial x_j}\right) \tag{5}$$

where, Pr_t is the turbulent Prandtl number, and $\mu_t = \rho \frac{a_1 k}{max(a_1\omega\,,\, S\,F_2)}$ is the eddy viscosity, and S is the vorticity magnitude.

The turbulent kinetic energy equation k is given as:

$$u_i \frac{\partial(\rho k)}{\partial x_i} = \tau_{ij}\frac{\partial u_i}{\partial x_j} - \beta^*\rho\omega k + \frac{\partial}{\partial x_j}\left((\mu + \sigma_k\mu_t)\frac{\partial k}{\partial x_j}\right) \tag{6}$$

The specific dissipation rate ω is given as:

$$u_i \frac{\partial(\rho\omega)}{\partial x_i} = \frac{\gamma}{\upsilon_t}\tau_{ij}\frac{\partial u_i}{\partial x_j} - \beta\rho\omega^2 + \frac{\partial}{\partial x_j}\left[(\mu + \sigma_\omega\mu_t)\frac{\partial\omega}{\partial x_j}\right] + 2\rho(1-F_1)\sigma_{\omega 2}\frac{1}{\omega}\frac{\partial k}{\partial x_j}\frac{\partial\omega}{\partial x_j} \tag{7}$$

where, γ, a_1, β, β^*, σ_k, σ_ω, and $\sigma_{\omega 2}$ are closure coefficient and F_1, F_2 are blending functions. More details about these parameters can be found in the study [14].

Most HXs operate for long periods. Thus, they can be modeled as steady-flow devices. As such, the values of the inlet velocities and temperature remain the same. Also, the specific heat of the cold and hot fluids changes with temperature. However, an average value over the range of temperatures can be considered. The heat transfer occurs only between the two fluids, and the heat transfer to the surrounding is negligible and thus can be modeled as an insulated surface. Therefore, from the first law of thermodynamics, the rate of heat transfer can be calculated as:

$$\dot{Q} = \dot{m}_c\, c_{pc}\left(T_{c,\,out} - T_{c,\,in}\right) \text{ or } \dot{Q} = \dot{m}_h\, c_{ph}\left(T_{h,\,in} - T_{h,\,out}\right) \tag{8}$$

where, $\dot{m}_c$ and $\dot{m}_h$ are the mass flow rates of the cold and hot fluids, respectively. c_{pc} and c_{ph} are the specific heats for the cold and hot fluids, respectively. T is the fluid temperature, and the subscripts h and c indicate the hot and cold fluids, respectively. The heat transfer rate can also be calculated as:

$$\dot{Q} = U\, A\, \Delta T_{lm} \tag{9}$$

where, $U = \frac{1}{h_i A_i} + R_{wall} + \frac{1}{h_o A_o}$ is the overall heat transfer coefficient, and R_{wall} can be ignored if the thickness of the walls of the HX is small and the material's thermal conductivity is high. A is the area of heat transfer, ΔT_{lm} is the log mean temperature difference, and it is defined as:

$$\Delta T_{lm} = \frac{\Delta T_1 - \Delta T_2}{\ln(\Delta T_1/\Delta T_2)} \tag{10}$$

where, ΔT_1 and ΔT_2 are the temperature differences between the inlet and outlet of the two fluids, as seen in Figure 1.

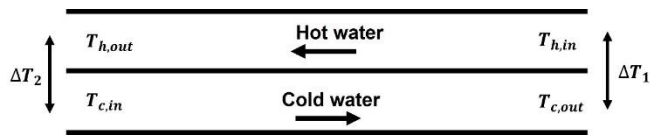

Figure 1. Log-mean temperature difference

The Reynold number formula is used to estimate the flow regime inside the polymer HX, and it is given as follows:

$$Re = \frac{\rho V D}{\mu} \quad (11)$$

where, D is the hydraulic diameter of the HX.

The average Nusselt number inside the HX can be calculated using the following equation:

$$Nu = \frac{hD}{k} \quad (12)$$

where, h is the convective heat transfer coefficient, k is the thermal conductivity of the water, and D is the hydraulic diameter of the HX.

2.1 Geometry

Additive manufacturing made it possible to manufacture complex geometries. This feature of 3D printing can be utilized in designing and fabricating HXs. Currently, polymer-based 3D printing is relatively cheap and accessible. At the same time, precise metal-based 3D printing is expensive and not easily accessible. However, some companies and Universities offer metal 3D printing services without needing costly printers. However, CFD has good potential in modeling the flow and heat transfer in the complex shapes of the HXs before physical printing and testing. The geometry presented here can be manufactured with conventional means. However, the main idea is to test the feasibility of 3D-printed polymer-based materials in the design of HX using CFD. If proven feasible, complex shapes can be further studied.

The proposed additively manufactured polymer-based HX is modeled using Ansys Fluent. The flow field inside the channels is resolved to study the thermal-hydraulic performance. There are two primary geometries used in the simulations. The first one is a flat plate HX. The second one is a corrugated plate HX. The geometry of both HXs is given in Figure 2. The main idea of the corrugated HX is to introduce turbulence for better heat transfer enhancement and not to have excessive pressure drop. The corrugations are given as semi-circular shapes along the HX surface. The semi-circular shapes are built with four different diameters. Also, the semi-circular shapes are arranged in three different pitches. Notably, the semi-circular shapes in one channel make a pocket-like shape in the adjacent channel. So, a series of protrusions and pockets are arranged in each channel that makes the HX.

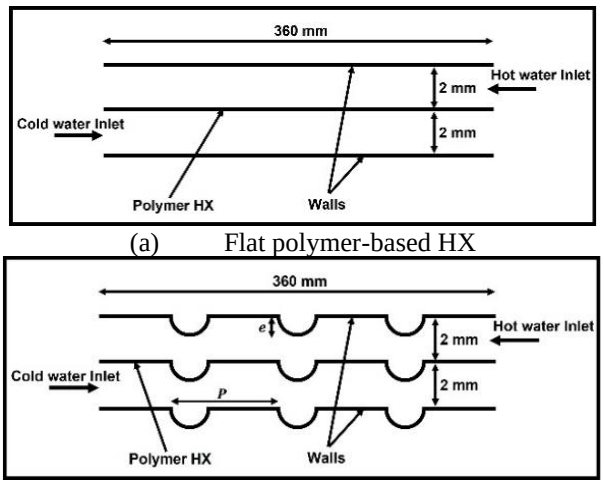

Figure 2. Schematic diagrams for the proposed polymer-based HX

2.2 Numerical model

To better understand the effect of different parameters on the performance of the HX. The simulations are made with varying flow rates, giving Reynold's numbers of 1200, 1500, 2000, 2500, and 3000. The characteristic length of the height of the semi-circular shape is variable and equal to e/D=0.25, 0.375, 0.5, and 0.625 where D is the hydraulic diameter of either the hot or the cold channel. The distance between the semi-circular shapes in the streamwise direction was varied as P=10, 13, and 16 mm. Other shapes for the corrugations can easily be modeled as well, but the semi-circular shape was chosen for its simplicity. The main idea of using a semi-circular shape is to test the validity of 3D-printed polymer-based material to construct HXs. However, metal 3D printing is feasible but expensive.

The simulations in this study are assumed to be steady state, and no initial condition is given other than the standard initialization to run the steady state simulations. The inlet boundary condition is velocity inlet, and the average velocity at the inlet section is calculated based on the Reynold numbers mentioned above and equation (Eq. (11)). The outlet boundary condition is a pressure outlet with zero-gauge pressure. The polymer surface separating the cold and hot fluids has coupled boundary conditions modeled according to (Eq. (8)). The hot and cold channels' top and bottom surfaces are modeled as insulated surfaces or surfaces with zero heat flux.

A SIMPLE scheme was used in the pressure velocity coupling. A second-order scheme was used for the spatial discretization of the pressure equation, and a second-order upwind for momentum, turbulent kinetic energy, specific dissipation rate, and energy equations.

2.3 Mesh study

All the given geometries are meshed using Ansys fluent meshing software. The nature of the geometry makes the number of elements high, and a high-performance computer (HPC) is needed to perform the simulations. An unstructured mesh was used to mesh the geometries in the semi-circular shape case. At the same time, a structured mesh was used for the flat plate heat exchanger case. The mesh near the heat transfer walls is made fine enough to capture the thin thermal and velocity boundary layers. Figure 3 (a) shows a snapshot of the mesh used in the simulations for the corrugated cases.

A mesh study was performed on the semi-circular shape plate heat exchanger. Six types of meshes were used, M1 to M6. Where Table 1 shows the details of the mesh used in the simulations. All the mesh study cases were set with a Reynolds number of 3000, a wall thickness of t=0.5 mm, seven automatic inflation layers, and with counter flow arrangement. The k-ω SST model is used in the mesh study. All simulations had a residual of less than 1e-3. A SIMPLE scheme was used for the pressure-velocity coupling and a second-order upwind for all the transport equations.

Figure 3 (b) shows the results of the mesh study. To conclude a mesh-independent status, the friction factor in either channel of the HX was calculated. As shown in Figure 3 (b), the friction factor converges to around the value of 2.2 for the mesh count of 250,000 elements. Also, the value of the friction factor with the 128,000 elements is close to the 250,000-mesh element. Therefore, the 128,000 elements case was chosen in the rest of the simulations.

Table 1. Details of the mesh elements and the y^+ values for the six different meshes used in the mesh-independent study

Mesh	M1	M2	M3	M4	M5	M6
Count	10,000	26,000	49,000	78,000	128,000	245,000
y^+	1.35	1.66	1.21	0.91	0.64	0.42

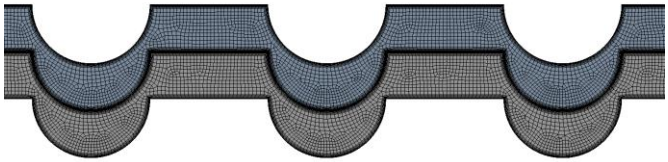

(a) Mesh used in the simulations

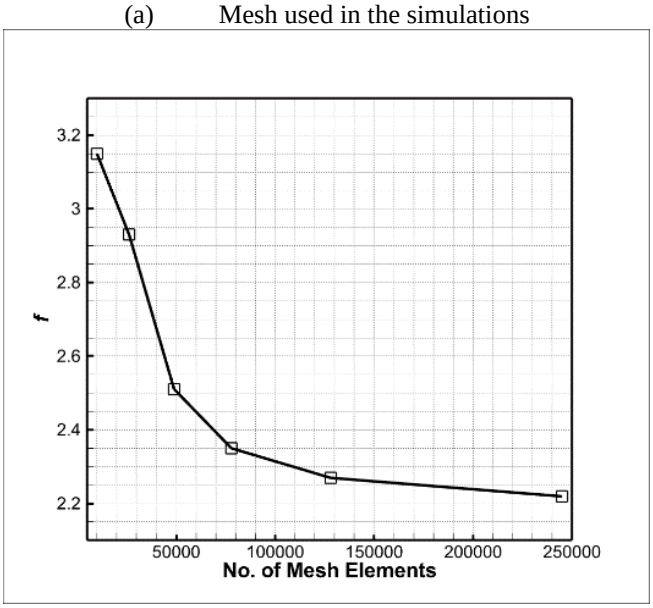

(b) Friction factor with the number of mesh elements

Figure 3. Mesh study

2.4 Validation

The CFD model was validated with existing experimental work from the literature [15]. Their experiment uses a water-to-water plate heat exchanger with corrugations to investigate the convective heat transfer coefficient. The plate heat exchanger consisted of two flow channels and three plates with a counter-flow arrangement. The corrugations made in the plates are chevron-type corrugations with an angle of 30° and 60°. The water was circulated in the flow channels so that the Reynold number is between 500 and 2500. Figure 4 (a) shows the geometry used to validate the model with the experiment. A 3D geometry was used to capture the primary and secondary flows in the validation. The corrugations made in the geometry were set to a chevron angle of 60°. The validation results are shown in Figure 4 (b), where the average Nusselt number in the reported results of the experiment is compared with the average Nusselt number from the CFD model. The results show a good match between the experimental results and the CFD model. Therefore, the CFD model can be considered validated.

The thermal conductivity of polymer-based materials is low compared with metals such as aluminum. The well-known polylactic acid material (PLA) that is widely used in desktop 3D printers has a low thermal conductivity and a low melting temperature point. However, the development of new filaments is rapidly evolving, and new types of filaments appear in the market regularly. One of the interesting new polymer-based filaments is the one produced by (TCPOLY) under Ice9^{TM} [16]. As indicated by the technical data sheet for the filament, the material is thermally conductive and electrically non-conducting. The reported thermal conductivity is 6 W⁄(m·K), the density is 1400 kg⁄m^3, the specific heat is 1300 J⁄(kg·K), and the maximum continuous temperature is 110℃. The properties of this material are used in the CFD simulations of this study as the polymer-based material.

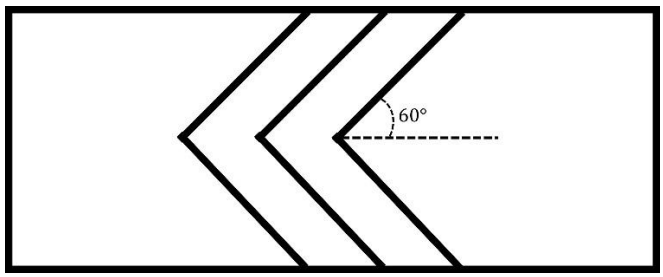

(a) Validation geometry schematic diagram

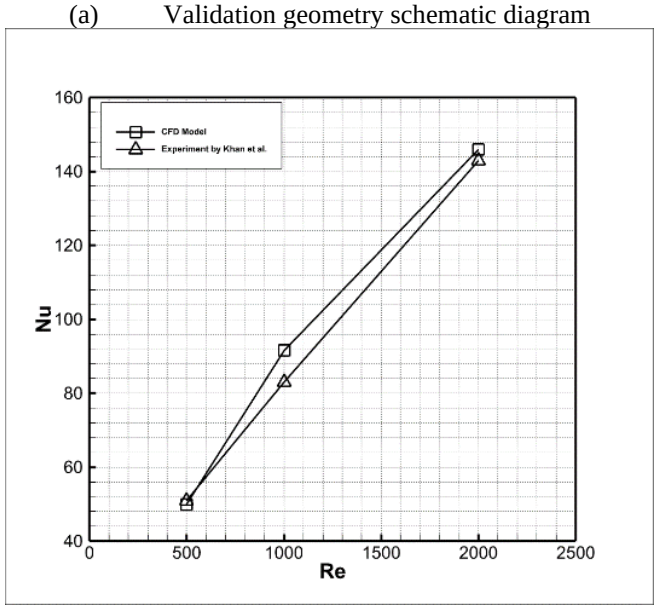

(b) Validation results

Figure 4. Validation results for the CFD model with the experimental work

3. RESULTS AND DISCUSSION

One of the essential results in the design of any HX is the pressure drop that develops during the operation. The introduction of the corrugations inside the HX enhances the thermal performance of the HX but the pumping power increases. Figure 5 shows the results of the simulations and how the friction factor changes with the different parameters.

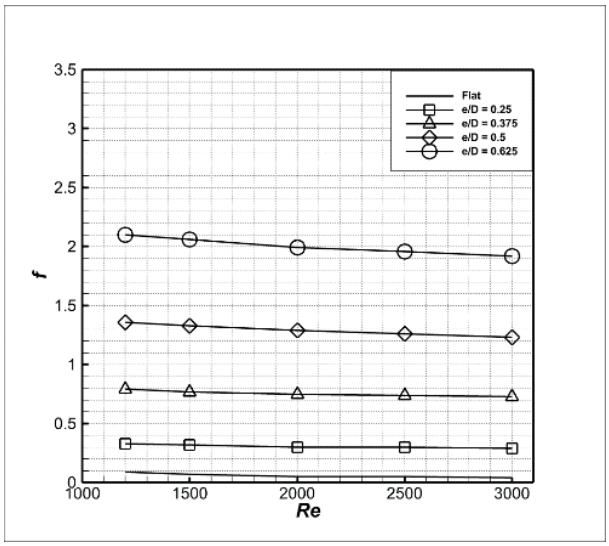

(a) P = 10 mm

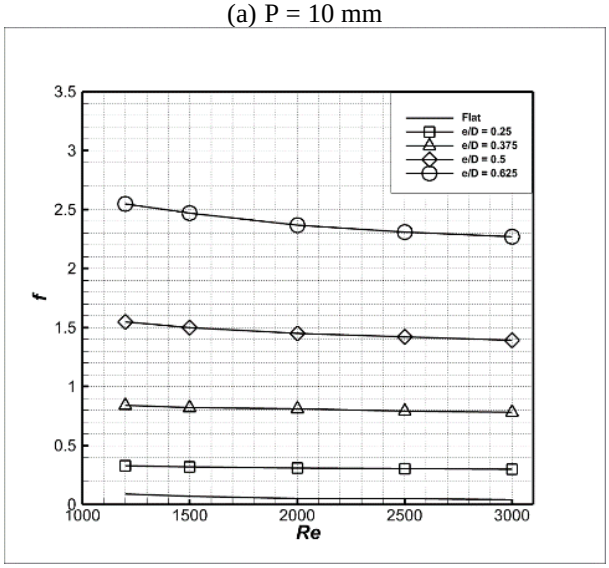

(b) P = 13 mm

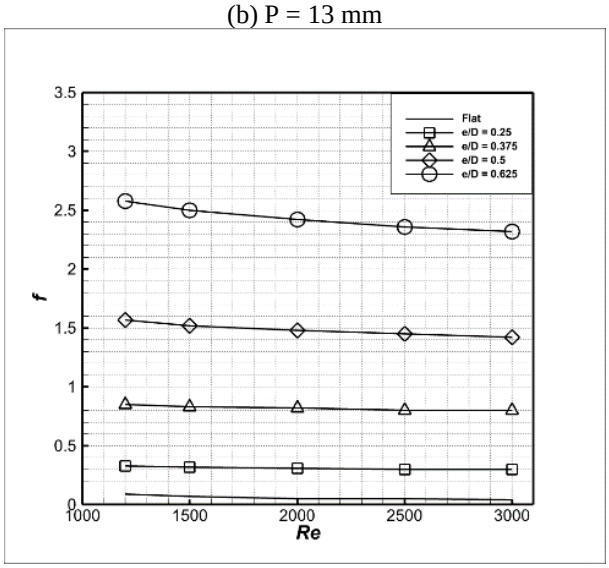

(c) P = 16 mm

Figure 5. Friction factor inside either the hot or cold side of HX

It is apparent from the results presented in Figure 5 that the friction factor has the lowest values when there are no corrugations present inside the HX. The introduction of semi-circular corrugations increases the friction factor inside the HX. As the height of the corrugations is increased, the friction factor increases.

Figure 5 (a) shows the friction factor inside the HX for tightly spaced corrugations, namely P = 10 mm. For the highest value of *e/D*, the friction factor is the greatest. As the corrugation height decreases, the friction factor also decreases. However, for the same *e/D* case, the friction factor decreases slightly and is almost constant with Reynold's number.

Figure 5 (b) and (c) show the same trend as Figure 5 (a). However, the friction factor values increase as the spacing between successive corrugations increases.

The trend of the friction factor shown in Figure 5 is identical to the well-known Moody chart. In a typical Moody chart, the friction factor values with the Reynold number in rough pipes with a wholly turbulent flow are independent of the Reynold number. This trend in the results is reassuring and can be considered as another validation for the results of the simulations presented in this study.

Figure 6 shows the results of the average Nusselt number inside the HX as a function of the Reynold number for different heights of corrugations. Figure 6 (a) shows the Nusselt number variations for P = 10 mm. As expected, the flat HX case has the lowest values of the Nusselt number. As the corrugation's height increases, the Nusselt number value increases. Also, the Nusselt number increases linearly with the increase of Reynold's number. It is to be noted that the gap between the values of the Nusselt number for the flat case and the corrugation is high, especially at high Reynold numbers. This gap suggests that even any small corrugations in the HX will give good mixing and high values of Nusselt number.

Figure 6 (b) and (c) show a similar trend in the average Nusselt number results for P = 13 and 16 mm, respectively. However, the average Nusselt number values are higher in each case. Thus, tightly spaced corrugations are not beneficial for the average Nusselt number.

Figure 7 shows the overall thermal-hydraulic performance of polymer HX. As the corrugations are introduced inside the HX, the average Nusselt number increases at the expense of the pumping power. To better understand the gain in increasing the average Nusselt number with friction factor, the thermal-hydraulic performance is used as an index to justify the addition of the corrugations. A value for the thermal-hydraulic performance greater than unity indicates that the average Nusselt number increase is beneficial, and the added pumping power is justified. As the value for the thermal-hydraulic performance increases, the polymer heat exchanger's performance will improve.

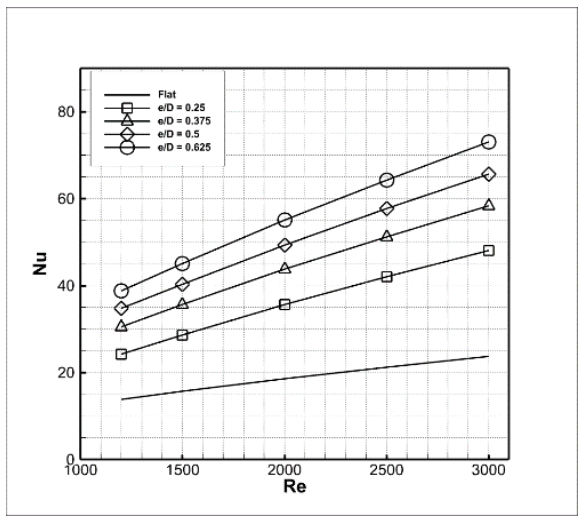

(a) P = 10 mm

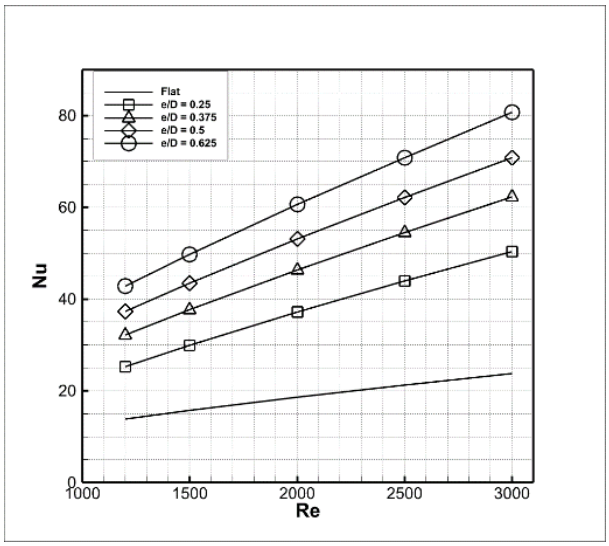

(b) P = 13 mm

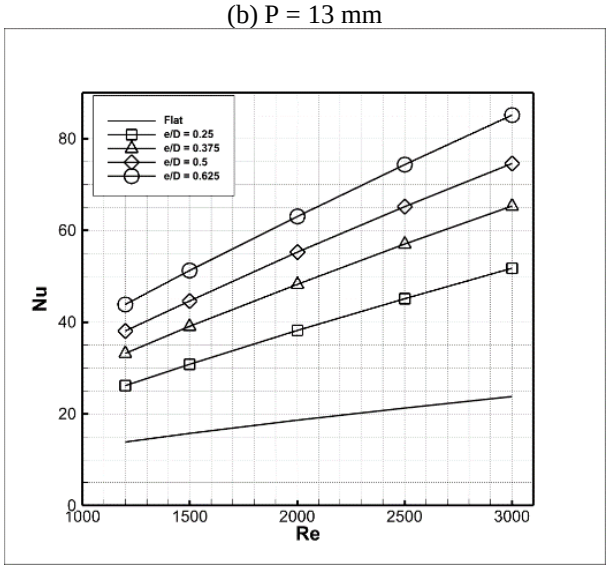

(c) P = 16 mm

Figure 6. Nusselt number for the HX

All the sub-figures in Figure 7 show the same general trend for thermal-hydraulic performance. The small corrugation (e/D)=0.25 inside the HX had a better performance than the large corrugations (e/D)=0.625. For P=10 mm, the (e/D)=0.25 corrugations had a 19% enhancement in the thermal-hydraulic performance at a Re=1200 compared to (e/D)=0.625. The enhancement in the thermal-hydraulic performance is 16% and 19% for P=13 and 16 mm, respectively at Re=1200. Also, the thermal-hydraulic performance decreases with increasing the Reynold number, which stays at almost a constant value for the higher Reynold numbers. As the pitch of the corrugation is further spaced, the thermal-hydraulic performance is enhanced. The thermal-hydraulic performance is calculated based on the following equation taken from [17]:

$$THP = \frac{\left(\frac{Nu}{Nu_S}\right)}{\left(\frac{f}{f_S}\right)^{\frac{1}{3}}} \tag{13}$$

Figure 8 compares flat HX between polymer-based HX and an aluminum HX. The same thickness for the HX was used in both cases. The use of aluminum HX is superior to polymer-based HXs since the thermal conductivity of aluminum is higher than any polymer material. However, when the thickness of the polymer HX is thin, the heat transfer rate in the HX can be good enough for some applications.

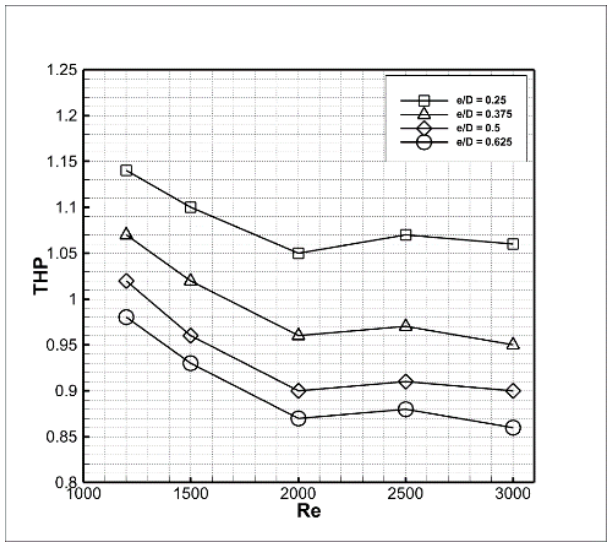

(a) P = 10 mm

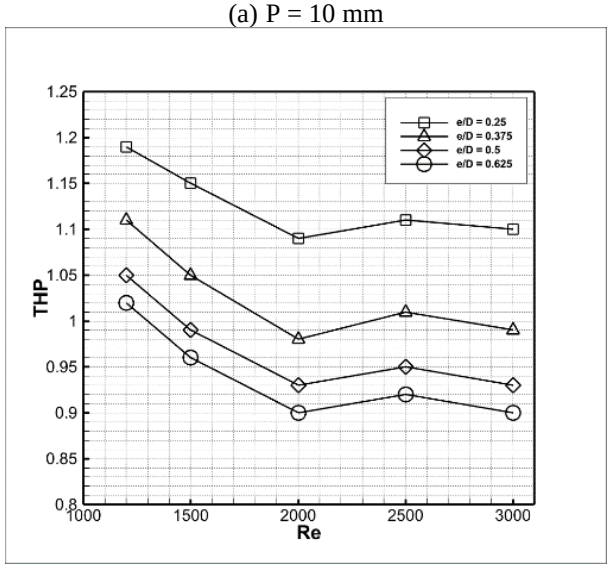

(b) P = 13 mm

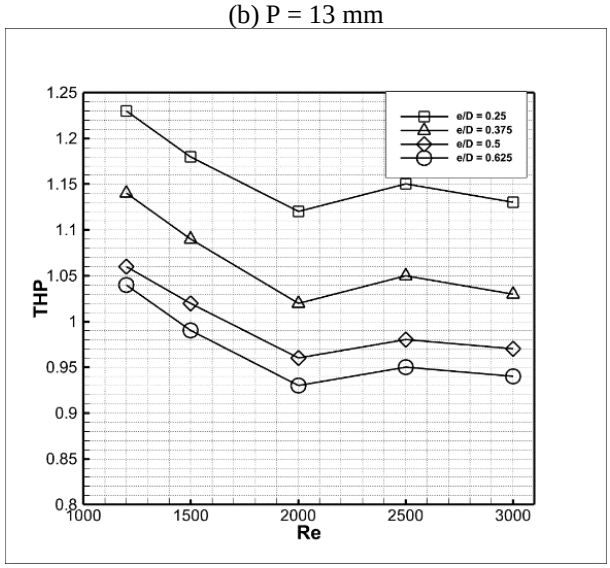

(c) P = 16 mm

Figure 7. Thermal-hydraulic performance for the HX

Figure 8 shows that for a HX with a thickness of 0.5 mm the average Nusselt numbers are not far from each other. The results show that the difference in the average Nusselt number

between polymer-based HX and Aluminum HX is small at low Reynold numbers. However, as the Reynold number increases, the difference in the average Nusselt number between polymer-based HX and Aluminum HX is larger. These results might indicate that polymer-based HX is preferable at low Reynold numbers if the polymer is needed as an HX material. However, at high Reynold numbers, aluminum-based HX is better.

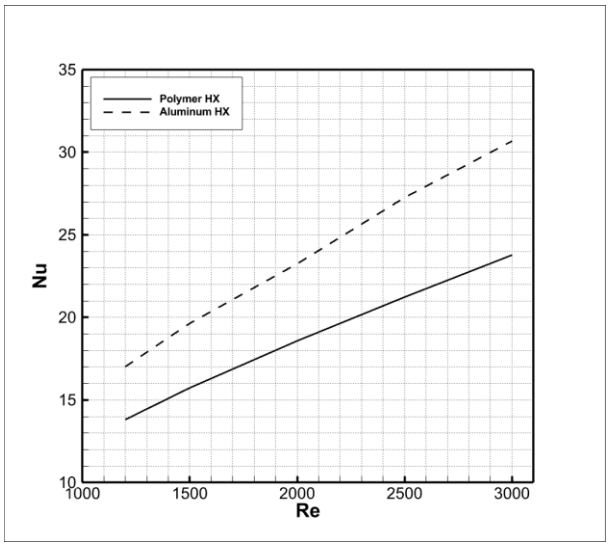

Figure 8. The average Nusselt number with Reynold number in a flat heat exchanger with different materials for the HX, polymer, and aluminum

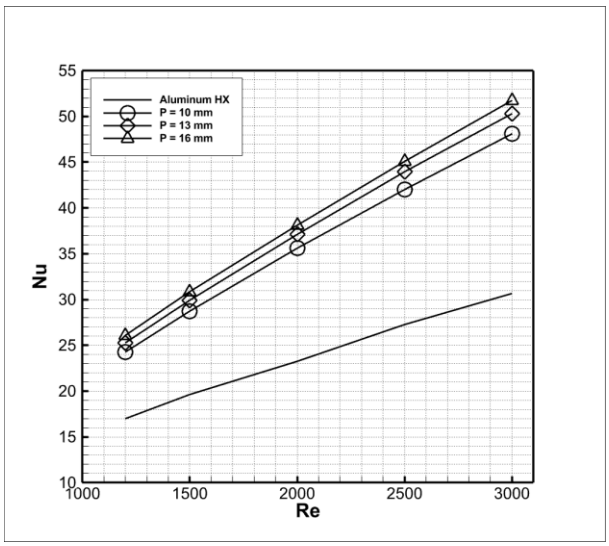

Figure 9. Comparing the average Nusselt number for flat Aluminum HX with polymer-based heat exchangers for corrugation height of e/D=0.25 at different pitch spacings for an HX thickness of 0.5 mm

Figure 9 compares the average Nusselt number with the Reynold number for flat aluminum-based HX and corrugated polymer-based HX. Both HXs have a thickness of 0.5 mm. This comparison sheds light on the possibility of using corrugated polymer-based HX for low-temperature applications. The thickness of the corrugations in the polymer-based HX is e/D=0.25.

From Figure 9, the average Nusselt number in the polymer-based HX is higher than the flat aluminum HX. The difference in the average Nusselt number between aluminum and polymer-based HXs is small at low Reynold numbers. The difference in the average Nusselt number between the corrugated polymer-based HXs and the flat aluminum HX is high at high Reynold numbers. These interesting results indicate that using polymer-based HXs with corrugations is more beneficial for heat transfer than using flat aluminum-based HX. Of course, aluminum-based HX is mechanically more robust and can withstand high temperatures without degradation.

From Fourier's law of heat conduction, the rate of heat transfer depends on the temperature difference across the material, the material type, and the thickness of the material according to the one-dimensional form as $q_x=-k\,dT/dx$. In the case of plate HXs, the comparison is between two types of materials. Aluminum has a thermal conductivity of around 202 W/(m·K) is compared with a polymer material that has a thermal conductivity of 6 W/(m·K). Aluminum is superior to polymer when it comes to thermal conductivity. However, this section of the results discusses the effect of adding corrugations to the polymer-based HX and to be compared it with a flat aluminum HX. Adding the corrugations to the polymer-based HX will help increase the convective heat transfer and might supersede the high thermal conductivity of the aluminum.

Figure 10 shows the average Nusselt number as the thickness of the HX is varied from 0.5 mm to 3.0 mm at a Reynold number of 3000 for the flat aluminum and the corrugated polymer HX.

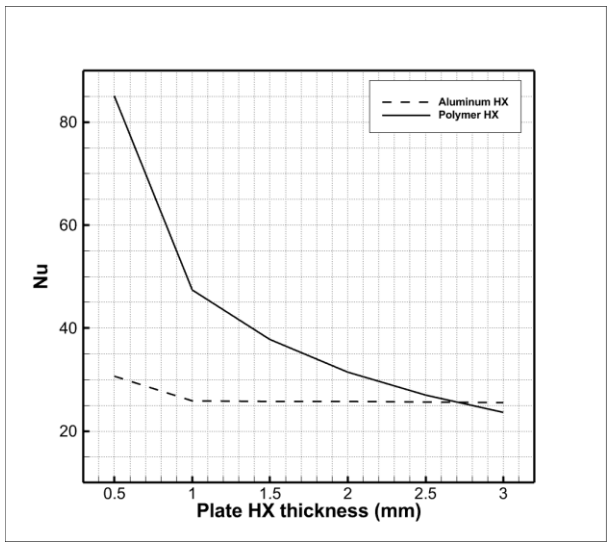

Figure 10. Comparing the average Nusselt number versus the plate HX thickness for flat aluminum HX with polymer-based heat exchanger containing corrugations with P = 16 mm and e/D=0.625 and a Re=3000

The results show that at a thickness of 0.5 mm the Nusselt number in the corrugated polymer HX is almost three times higher than the flat aluminum HX. As the thickness of the plate HX is increased to 1.0 mm the average Nusselt number drops drastically in the corrugated polymer HX. The same behavior is observed with the flat aluminum HX, but the average Nusselt number reduction is small. The corrugated polymer HX at a thickness of 1.0 mm still has a higher average Nusselt number than the flat aluminum HX. As the HX thickness is increased from 1.0 mm to 3.0 mm, the average Nusselt number in the flat aluminum HX is slowly decreasing and is almost

constant. The average Nusselt number in the corrugated polymer HX is reducing linearly as the thickness of the HX is increased from 1.0 mm to 3.0 mm. At around 2.7 mm of HX thickness, the conduction resistance in the polymer HX increases, which reduces the heat transfer rate inside the polymer HX. Therefore, the average Nusselt number in the flat aluminum HX is becoming better than the corrugated polymer HX after 2.7 mm of HX thickness.

The addition of the corrugations enhances the convective heat transfer in HXs and increases the average Nusselt number. We must look closely at how the corrugations enhance the heat transfer inside HXs.

Figure 11 shows the local variations of temperature along the surface of the corrugated HX at the hot side of the HX. From Fourier's law of heat conduction, the heat transfer rate increases as the temperature difference between the hot and cold sides increases. However, as the fluid passes through the hot side of the HX, the average temperature decreases along the length of the HX and especially near the cold side wall. The hot fluid far away from the cold side wall has a higher temperature at the same streamwise location.

The addition of corrugations allows the mixing of the fluid in the hot channel, which increases the average fluid temperature near the cold side wall. Therefore, the rate of heat transfer increases compared with the flat cases.

Figure 11 shows the temperature variation along the streamside direction. The direction of the flow is from right to left. As the water enters the hot side of the HX, naturally, the water is cooled because of the heat exchange with the cold water. Therefore, the temperature of the hot water decreases. The addition of corrugations helps in momentum mixing. The mixing brings the hot fluid far away from the HX surface and mixes it with the cold fluid. The presence of the corrugations makes the temperature almost constant. As the fluid clears from the corrugations, the temperature drops. As the temperature profile for the corrugated case is compared with the flat case, the flat case has a high thermal boundary layer growing along the streamwise direction, reducing heat transfer. The corrugation breaks the thermal boundary layer over the HX surface.

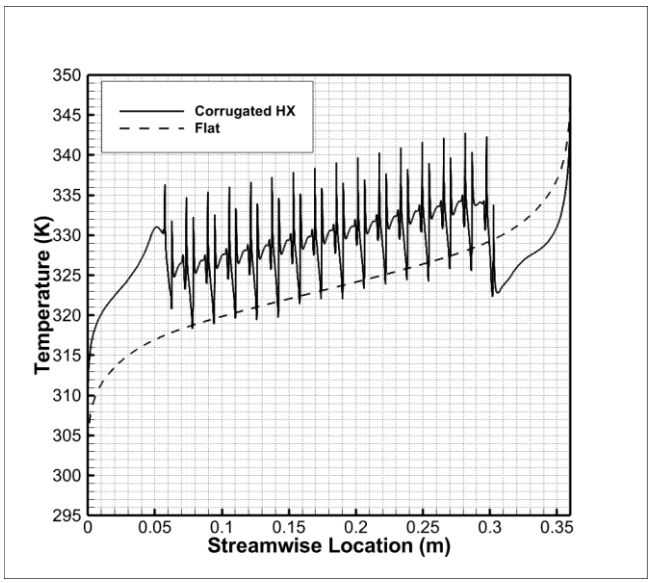

Figure 11. Comparison between the temperature profiles along the surface of the HX in the hot side from inlet to outlet for the corrugated case *e/D*=0.625 and P=16 mm, and Re=3000 and the flat case with Re=3000

4. CONCLUSION

This paper discussed the possibility of using polymer-based materials in the design of heat exchangers. Typically, heat exchangers are made of highly conductive materials for a better heat transfer rate. However, with the advent of additive manufacturing and the widespread use of 3D printers, using polymer materials in the design of heat exchangers might be helpful.

The thermal conductivity of polymer materials is generally low and cannot be compared with most metal materials. However, some new polymer-based materials have a higher thermal conductivity than regular polymers that can be used in the design of heat exchangers.

Using a polymer-based heat exchanger is explored using computational fluid dynamics simulations. Ansys fluent is used as the CFD tool in all the results obtained. The main objective of this paper was to study the effect of 3D polymer printed HXs and how the heat transfer rate can be increased using mixing promoters (corrugations) and be compared with aluminum HXs.

Two-dimensional geometry is used to conduct the simulations. It was made sure that the results obtained from the CFD simulations were mesh independent. Also, the model was validated against an existing experimental result from the literature. The results showed good agreement with the experiment, and the CFD model is considered validated.

The main results of the CFD simulations show an excellent prospective for using polymer materials in heat exchangers. The heat exchanger surface should be as thin as possible to reduce the conduction thermal resistance. Also, corrugations should be used to enhance the rate of heat transfer. The corrugation height should not be high to avoid the high pumping power related to the increase in the friction factor. From the analysis of the thermal-hydraulic performance, high thermal-hydraulic performance is achieved as the pitch of the corrugations is increased, and the height of the corrugations is decreased with a low flow rate.

When the corrugated polymer-based heat exchanger is compared with the flat aluminum heat exchanger, the corrugated polymer-based heat exchanger performs better when the thickness of the heat exchanger surface is less than 2.7 mm. After that, aluminum HX is superior.

It is to be noted that polymer-based heat exchangers will have a limited temperature range of operation (110℃) since the polymer materials will not withstand high temperatures. However, 3D printers are becoming cheap and widely available so 3D-printed heat exchangers can be used in many special applications.

Also, the study has several limitations, namely, that it is two-dimensional. Turbulent fluid flow is complex, and fluid flows are three-dimensional. The geometry presented here is two-dimensional and secondary flows are not resolved. All the cases are simulated as steady-state cases, and fluids are transient. However, high computing power is needed to produce transient and fully turbulent results.

Many practical complications may arise with 3D-printed heat exchangers, such as materials degradation and liquid leakage between the 3D-printed layers. Future work suggests that experiments are needed to ensure that 3D-printed heat exchangers can handle liquid-to-liquid heat transfer without mixing from the leakage between the layers. Also, the research could be pointed toward developing new polymer materials with high thermal conductivity and endurance. Furthermore,

CFD simulations using 3D geometry might be necessary to understand the flow field inside the HX better. Several unique corrugations might be used in the 3D polymer-based CFD simulations that might enhance the performance of 3D-printed HXs.

REFERENCES

[1] Cengel, Y.A. (2022). Heat Transfer a Practical Approach. Second Edi. Mcgraw-Hill.

[2] Gendera, M., Ludwig, W. (2023). CFD modelling of pressure drop in double-pipe heat exchanger with turbulators using a porous media model. International Journal of Heat and Technology, 41(1): 162-170. https://doi.org/10.18280/ijht.410117

[3] Abdulrasool, A.A., Aljibory, M.W., Abbas, A.K., Al-Silbi, M.M. (2023). A computational study of perforated helical tube inserted in a double pipe heat exchanger with fluid injection. International Journal of Heat and Technology, 41(1): 35-45. https://doi.org/10.18280/ijht.410104

[4] Wang, Q., Chen, G., Zeng, M., Chen, Q., Peng, B., Zhang, D., Luo, L. (2010). Shell-side heat transfer enhancement for shell-and-tube heat exchangers by helical baffles. Chemical Engineering Transactions, 21: 217-222. https://doi.org/10.3303/CET1021037

[5] Wang, Y., Blache, R., Xu, X. (2017). Selection of additive manufacturing processes. Rapid Prototyping Journal, 23(2): 434-447. https://doi.org/10.1108/RPJ-09-2015-0123

[6] Haertel, J.H., Nellis, G.F. (2017). A fully developed flow thermofluid model for topology optimization of 3D-printed air-cooled heat exchangers. Applied Thermal Engineering, 119: 10-24. https://doi.org/10.1016/j.applthermaleng.2017.03.030

[7] Kim, J., Yoo, D.J. (2020). 3D printed compact heat exchangers with mathematically defined core structures. Journal of Computational Design and Engineering, 7(4): 527-550. https://doi.org/10.1093/jcde/qwaa032

[8] Lowrey, S., Hughes, C., Sun, Z. (2021). Thermal-hydraulic performance investigation of an aluminium plate heat exchanger and a 3D-printed polymer plate heat exchanger. Applied Thermal Engineering, 194: 117060. https://doi.org/10.1016/j.applthermaleng.2021.117060

[9] Puttur, U., Ahmadi, M., Ahmadi, B., Bigham, S. (2022). A novel lung-inspired 3D-printed desiccant-coated heat exchanger for high-performance humidity management in buildings. Energy Conversion and Management, 252: 115074. https://doi.org/10.1016/j.enconman.2021.115074

[10] Ahmadi, B., Cesarano, J., Nawaz, K., Ninos, N., Bigham, S. (2023). A high-performance lung-inspired ceramic 3D-printed heat exchanger for high-temperature energy-efficient systems. Applied Thermal Engineering, 219: 119378. https://doi.org/10.1016/j.applthermaleng.2022.119378

[11] Laitinen, A., Saari, K., Kukko, K., Peltonen, P., Laurila, E., Partanen, J., Vuorinen, V. (2020). A computational fluid dynamics study by conjugate heat transfer in OpenFOAM: A liquid cooling concept for high power electronics. International Journal of Heat and Fluid Flow, 85: 108654. https://doi.org/10.1016/j.ijheatfluidflow.2020.108654

[12] Wang, G., Gu, Y., Zhao, L., Xuan, J., Zeng, G., Tang, Z., Sun, Y. (2019). Experimental and numerical investigation of fractal-tree-like heat exchanger manufactured by 3D printing. Chemical Engineering Science, 195: 250-261. https://doi.org/10.1016/j.ces.2018.07.021

[13] Hein, L.L., Mortean, M.V.V. (2021). Theoretical and experimental thermal performance analysis of an additively manufactured polymer compact heat exchanger. International Communications in Heat and Mass Transfer, 124: 105237. https://doi.org/10.1016/j.icheatmasstransfer.2021.105237

[14] Menter, F.R. (1994). Two-equation eddy-viscosity turbulence models for engineering applications. AIAA Journal, 32(8): 1598-1605. https://doi.org/10.2514/3.12149

[15] Khan, T.S., Khan, M.S., Chyu, M.C., Ayub, Z.H. (2010). Experimental investigation of single phase convective heat transfer coefficient in a corrugated plate heat exchanger for multiple plate configurations. Applied Thermal Engineering, 30(8-9): 1058-1065. https://doi.org/10.1016/j.applthermaleng.2010.01.021

[16] TCPOLY, Ice9 Flex TPU filament. https://tcpoly.com/purchase-ice9-materials/, accessed on Apr. 14, 2023.

[17] Dizaji, H.S., Jafarmadar, S., Mobadersani, F. (2015). Experimental studies on heat transfer and pressure drop characteristics for new arrangements of corrugated tubes in a double pipe heat exchanger. International Journal of Thermal Sciences, 96: 211-220. https://doi.org/10.1016/j.ijthermalsci.2015.05.009

NOMENCLATURE

Symbol	Definition	SI Units
A	Area of the heat transfer surface in the heat exchanger	m^2
c	Specific heat	$J/kg \cdot K$
D	Hydraulic diameter of the heat exchanger	m
e	Corrugations height	m
h	Convective heat transfer coefficient	$W/m^2 \cdot K$
k	Thermal conductivity	$W/m \cdot K$
$\dot{m}$	Water mass flow rate	kg/s
P	Streamwise pitch for the corrugations	m
$\dot{Q}$	Rate of heat transfer	W
R	Thermal resistance	K/W
T	Temperature	K
U	Overall heat transfer coefficient	$W/m^2 \cdot K$
ρ	Fluid density	kg/m^3
μ	Fluid viscosity	$N \cdot s/m^2$